Cloning and characterization of murine preproendothelin-1 gene and role of endothelin-1 in cardiovascular development

（マウスエンドセリン-1遺伝子のクローニングと構造、発現解析
及び心血管系の発生におけるエンドセリン-1の役割）

前村浩二

Cloning and characterization of murine preproendothelin-1 gene

Cloning and characterization of murine preproendothelin-1 gene and role of endothelin-1 in cardiovascular development

(マウスエンドセリン-1遺伝子のクローニングと構造、発現解析及び心血管系の発生におけるエンドセリン-1の役割)

前村　浩二

Abstract

Endothelin-1 (ET-1) is a 21-amino acid peptide with various biological activities including vasoconstriction and cell proliferation. Recently, gene targeting of the mouse of preproET-1 gene (*Edn1*) revealed that ET-1 is essential to the normal development of pharyngeal arch-derived tissues and organs. In the present study, I focused on the potential role of ET-1 in cardiovascular development. To clarify this, I first cloned and characterized the mouse *Edn1* gene and examined its expression in reference to development. *Edn1* comprises five exons and the open reading frame encodes for 202 amino acid preproET-1. The sequences and structural organization of *Edn1* are highly homologous to those of other species, especially in the terminal 200 bp sequences of 3'-noncoding region. Interspecific backcross mapping located *Edn1* in the central region of chromosomal 13, where a mouse mutation congenital hydrocephalus (*ch*) is also mapped. The highest expression of *Edn1* mRNA is detected in the lung in adult mice. *Edn1* expression and ET-1 peptide levels in the lung are progressively increased during the perinatal stage, whereas the expression of *Edn3*, a gene encoding ET-3, is reciprocally decreased. *In situ* hybridization confirmed ET-1 expression in the endothelium of the arch arteries and cardiac outflow tract and the endocardial cushion as well as in the epithelium of the pharyngeal arches suggesting the involvement of ET-1 in cardiovascular development.

Secondly, the role of ET-1 in cardiovascular development was further examined by analyzing the cardiovascular phenotype of

Edn1$^{-/-}$ homozygous mice. *Edn1*$^{-/-}$ homozygotes displayed aortic arch malformations and ventricular septal defect with abnormalities of the outflow tract. The frequency and extent of these abnormalities are increased by treatment with neutralizing monoclonal antibodies or a selective ET_A receptor antagonist BQ123, suggesting that maternal-derived circulating ET-1 may cause a functional redundancy through, at least partly, the ET_A receptor. At an earlier embryonic stage, formation of pharyngeal arch arteries and endocardial cushion is disturbed in *Edn1*$^{-/-}$ homozygotes.

Taken all the present results together, I conclude that ET-1 is involved in the normal development of the heart and great vessels as well as the pharyngeal-arch-derived craniofacial tissues Especially, ET-1 knockout mice may serve as a good model for human congenital heart diseases.

Introduction

Endothelin-1 (ET-1) is a potent vasoconstrictor peptide originally isolated from cultured media of porcine vascular endothelial cells (1). ET-1 comprises 21 amino acid residues including 4 cystein residues, forming 2 disulfide bonds. Three isopeptides (ET-1, 2 and 3) encoded by different loci constitute a gene family (2) and act on two distinct G protein-coupled receptors (ET_A and ET_B) with different affinities (3, 4). Similar to other hormones and neurotransmitters, ET-1 arises from the precursor polypeptide, i.e. preproET-1, through proteolytic processing. PreproET-1 (212 amino acids in human) is proteolytically cleaved to form a 38 amino acid big-ET-1. Conversion of the big ET-1 to mature ET-1 is the final key step in ET-1 peptide biosynthesis. This conversion has been postulated to be catalyzed by a putative endothelin converting enzyme-1 (ECE-1) (5). The production of ET-1 is mainly regulated at the level of gene transcription. Previous reports have shown that ET-1 gene expression is stimulated by thrombin (1), interleukin 1-α (6), transforming growth factor-β (7), insulin (8), Ca^{2+}-ionophore (1), 12-*O*-tetradecanoyl phorbol-13-acetate (TPA) (9) and flow-mediated shear stress (10, 11) in cultured vascular endothelial cells. Sequence analysis of the human ET-1 gene 5'-flanking region revealed the presence of AP-1 sites (9, 12), which is known to respond to protein kinase C activation (13), and some of the stimulating factors are thought to activate ET-1 gene transcription through AP-1 sites.

In addition to vasoconstrictive effects on vascular smooth muscle cells, ET-1 has various biological activities such as proliferative

effects on many kinds of cells, stimulation of nitric oxide and prostacyclin release from vascular endothelial cells, regulation of hormone release and modulation of central nervous activity (14). These effects of ET-1 suggest that ET-1 may participate in the regulation of cardiovascular homeostasis and the pathogenesis of cardiovascular disease such as hypertension, vasospasm and atherosclerosis (15-17). However, there has been little consensus about the physiological and pathophysiological importance of ET-1. Recently, we disrupted the mouse *Edn1* locus encoding ET-1 by gene targeting (18). The resultant mice homozygous for ET-1 null mutation represent morphological abnormalities of the pharyngeal-arch-derived craniofacial tissues and organs, indicating that ET-1 is essential to normal pharyngeal-arch development.

In mammalian craniofacial morphogenesis, mesenchyme constituting the pharyngeal arches stems mainly from neural crest cells. Cranial neural crest cells migrate to the pharyngeal arch region and differentiate into ectomesenchymal cells. Neural crest-derived ectomesenchymal cells interact with surface ectoderm, resulting in further differentiation into various tissues such as cartilage and dentine of the teeth (19, 20). *In situ* hybridization detected ET-1 gene expression in the epithelium of pharyngeal arches (18), suggesting that ET-1 may be involved in this epithelial-mesenchymal interaction. Neural crest cells are also required for normal cardiovascular development (21-23). Ectomesenchymal cells derived from cardiac neural crest migrate to pharyngeal arches 3, 4 and 6 and contribute to the aortic arch development and aorticopulmonary septation. Thus, I speculated that ET-1 may participate not only in

the craniofacial development but also in the cardiovascular development. In the present study, to clarify the potential role of ET-1 in cardiovascular development, I first characterized the gene coding mouse preproET-1, a precursor of ET-1, (*Edn1*). I determined the genomic structure and chromosomal location of *Edn1*, investigated the developmental expression of ET-1 in the cardiovascular system. Then, I focused on the phenotypic manifestations of *Edn1*$^{-/-}$ homozygous mice in the cardiovascular system to examine the possibility that ET-1 may also contribute to the embryonic cardiovascular development.

Materials and Methods

Cloning and sequencing of the mouse preproET-1 genomic and complementary DNA

The mouse preproET-1 gene (*Edn1*) fragment containing exon 1 to 5 was cloned from BALB/c mouse genomic library in EMBL3 (gift of K. Miyagawa) using synthetic oligonucleotide probes derived from the partial mouse *Edn1* cDNA sequence (24). Four positive clones were isolated and characterized by restriction endonuclease mapping. Restriction enzyme-digested DNA samples were subjected to Southern analysis using the synthetic probes. All hybridized fragments were subcloned into pBluescriptSK+ for further characterization and sequencing. The mouse *Edn1* cDNA was cloned by reverse transcription(RT)-PCR. PCR was done on the mouse lung cDNA using a GeneAmp PCR kit (Perkin Elmer Cetus). Sense (5'-TGCAGAATGGATTATTTTCCCGTG-3') and antisense (5'-TGAGTCAGACACGAACACTCCCTA-3') primers were deduced from the sequence of rat ET-1 cDNA (25). Thirty-five cycles (94°C for 1 min, 60°C for 1 min, 72°C for 1.5 min) were used to amplify 1.0 kb products, which were cloned into TA cloning vector (Invitrogen). DNA sequencing was performed with an ABI373A DNA sequencer according to the instructions provided by the manufacturer (Applied Biosystems).

Chromosomal mapping

Interspecific backcross progeny were generated by mating (C57BL/6J × *M. spretus*)F_1 females and C57BL/6J males as described

(26). A total of 205 N_2 mice were used to map the *Edn1* locus (see text for details). DNA isolation, restriction enzyme digestion, agarose gel electrophoresis, Southern blot transfer and hybridization were performed essentially as described (27). All blots were prepared with Hybond-N^+ nylon membrane (Amersham). The probe, a 1.0-kb *Eco*RI fragment of mouse cDNA, was labeled with [α-^{32}P]dCTP using a nick translation labeling kit (Boehringer Mannheim); washing was done to a final stringency of 0.8 × SSCP, 0.1% SDS at 65°C. Fragments of 8.2, 3.1 and 1.4 kb were detected in *Hin*dIII-digested C57BL/6J DNA and fragments of 5.8 and 4.7 kb were detected in *Hin*dIII digested *M. spretus* DNA. The presence or absence of the 5.8 and 4.7 kb *M. spretus*-specific *Hin*dIII fragments, which coseggregated, was followed in backcross mice.

A description of the probes and restriction fragment length polymorphisms (RFLPs) for the loci linked to *Edn1* including Friend MuLV integration site 1 (*Fim1*), and interleukin 9(*Il9*) has been reported previously (28). Recombination distances were calculated as described (29) using the computer program SPRETUS MADNESS. Gene order was determined by minimizing the number of recombination events required to explain the allele distribution patterns.

Northern blot analysis

The antisense RNA probe for *Edn1* was prepared from the linearized plasmid containing a 1.0 kb fragment of *Edn1* cDNA by transcribing with RNA polymerase in the presence of [α-^{32}P]UTP (Amersham). cDNA for mouse ET-3 (*Edn3* cDNA) were cloned by PCR

using oligonucleotide primers deduced from their rat homologues (30). Probes for *Edn3* were prepared from the plasmids containing 303 bp of mouse *Edn3* cDNA. Total cellular RNA was extracted from various tissues of littermates using RNAzol (BIOTEX). RNA samples were heat-denaturated in formamide, electrophoresed through 1.2% agarose/formaldehyde gels and transferred to Hybond-N nylon membrane (Amersham). The membranes were hybridized for 24 hr at 65°C in 50% formamide, 0.5% SDS, 6×SSC, 2.5 × Denhardt's solution, 0.25 mg/ml salmon sperm DNA and ^{32}P-labeled probes. Membranes were washed twice in 2 × SSC/0.1% SDS at 65°C for 15 min, twice in 0.1 × SSC/0.1% SDS at 65°C for 15 min, and exposed to Kodak X-OMAT AR film at -80°C. For comparison of mRNA levels, the membranes were subsequently rehybridized with ^{32}P-labeled glyceraldehyde 3-phosphate dehydrogenase (GAPDH) probe to determine an internal standard of total RNA content.

Enzyme-linked Immunosolvent Assay

For the measurement of the ET-1 levels, I used a sandwich-enzyme-linked immunoassay (ELISA) as previously described (31). This assay system also detects ET-2 and the crossreactivity is 160%. The crossreactivity of big ET-1 is 0.15%. The ET-3 levels were determined by ELISA kits purchased from International Reagents Corp. (Kobe, Japan) (32).

Whole mount in situ hybridization.

A 1.0 kb fragment of the mouse ET-1 cDNA was subcloned in pBluescriptSK+ and nonradioactive antisense RNA probes were

synthesized with digoxygenin-11-UTP (Boehringer). Whole-mount fixation and *in situ* hybridization were performed as described (33). Hybridized embryos or hearts were washed at high stringency, incubated with alkaline phosphatase-conjugated anti-digoxygenin antibody and stained with nitro blue tetrazolium and 5-bromo-4-chloro-3-indoyl phosphate. For sections, hybridized embryos were fixed in 4% paraformaldehyde, embedded in paraffin, serially sectioned and faintly stained with eosin.

ET-1-knockout Mice

ET-1 knockout mice were established by gene targeting (18). The animals were maintained on a light-dark cycle with light from 9:00 to 21:00 at 25°C. Mice were fed with a normal diet and water ad libitum. Mice heterozygous for *Edn1*$^{-}$ mutant allele with the genetic background of the 129Sv/J × ICR hybrid were mated. In some *Edn1*$^{+/-}$ heterozygous pregnants intercrossed with *Edn1*$^{+/-}$ heterozygous males, osmotic minipumps (Alzet model 1007D, Alza) containing anti-ET-1 monoclonal antibodies HPE37B11 (34) (0.11 mg per day per mouse) or ET_A antagonist BQ123 (35) (0.96 mg per day per mouse) were subcutaneously implanted at 5.5 to 8.5 days postcoitum (d.p.c.) to achieve continuous infusion for 7 days. HPE37B11 (IgG1 subtype) recognized the C-terminal region of ET-1, crossreacted with ET-2 and ET-3, and neutralized the pressor effect of intravenously administered ET-1 (1 nmol/kg of body weight) (data not shown). Continuous infusion of saline or monoclonal antibodies of the same IgG1 subtype, which recognize rat intercellular adhesion molecule (ICAM) but do not recognize mouse

ICAM, served as control experiments. The dose of BQ123 was sufficient for antagonizing the effect of ET-1 through ET_A receptors (36). Pregnant mice were sacrificed by cervical dislocation and the fetuses were dissected from uterine decidua. *Edn1*$^{-/-}$ homozygous fetuses were identified by their characteristic craniofacial abnormalities and genotypes were confirmed by Southern analysis of tail genomic DNA samples. The heart and great vessels of *Edn1*$^{-/-}$ homozygous fetuses were observed by stereoscopy. For histological examinations, hearts were excised, fixed in 4 % paraformaldehyde and embedded in paraffin. They were serially sectioned into 8μm sections and stained with haematoxylin-eosin. The terminology and diagnosis of the anomalies were principally based on the established descriptions (37).

Statistical analysis.

Quantitative values were expressed as mean ± SEM. Student's *t* test was used to determine significant differences. Statistical comparison used χ^2 test. A value of $P<0.05$ was considered significant.

Results

Characterization of the mouse preproET-1 gene

I isolated four positive clones from a BALB/c mouse genomic library in EMBL3. Restriction endonuclease mapping indicated that all the clones were overlapping and the lengths of expected restriction fragments were identical to those of positive bands in genomic Southern blot hybridization. λE10, a clone which spanned the whole length of *Edn1*, was further characterized. *Edn1* cDNA fragments encompassing the whole open reading frame and a part of 3'-noncoding region were also cloned by RT-PCR to confirm the exon-intron structure of *Edn1*. The structure of *Edn1* was compared with that of the human preproET-1 gene which was reported previously (9, 38).

Edn1 is organized into five exons distributed over approximately 6.0 kb (Fig. 1). In the 5'-flanking region, a TATAAA sequence and a CAAT sequence were found at position -31 and -95, respectively. The structural organization of *Edn1* is very similar to that of the human preproET-1 gene with respect to number and size of the exons and introns. The first exon contains the 5'-noncoding region and 64 bp of the coding region. Twenty-one amino acid mature ET-1 is encoded in the second exon, whereas 39 amino-acid 'big ET-1', an intermediate product of ET-1 processing, is encoded over the second and third exons. ET-like peptide sequence containing 4 cysteine residues was also found in the third exon. The 3'-noncoding region encoded in the fifth exon is AT-rich and contains three ATTTA mRNA instability sequences within 150 bp upstream to the AATAAA

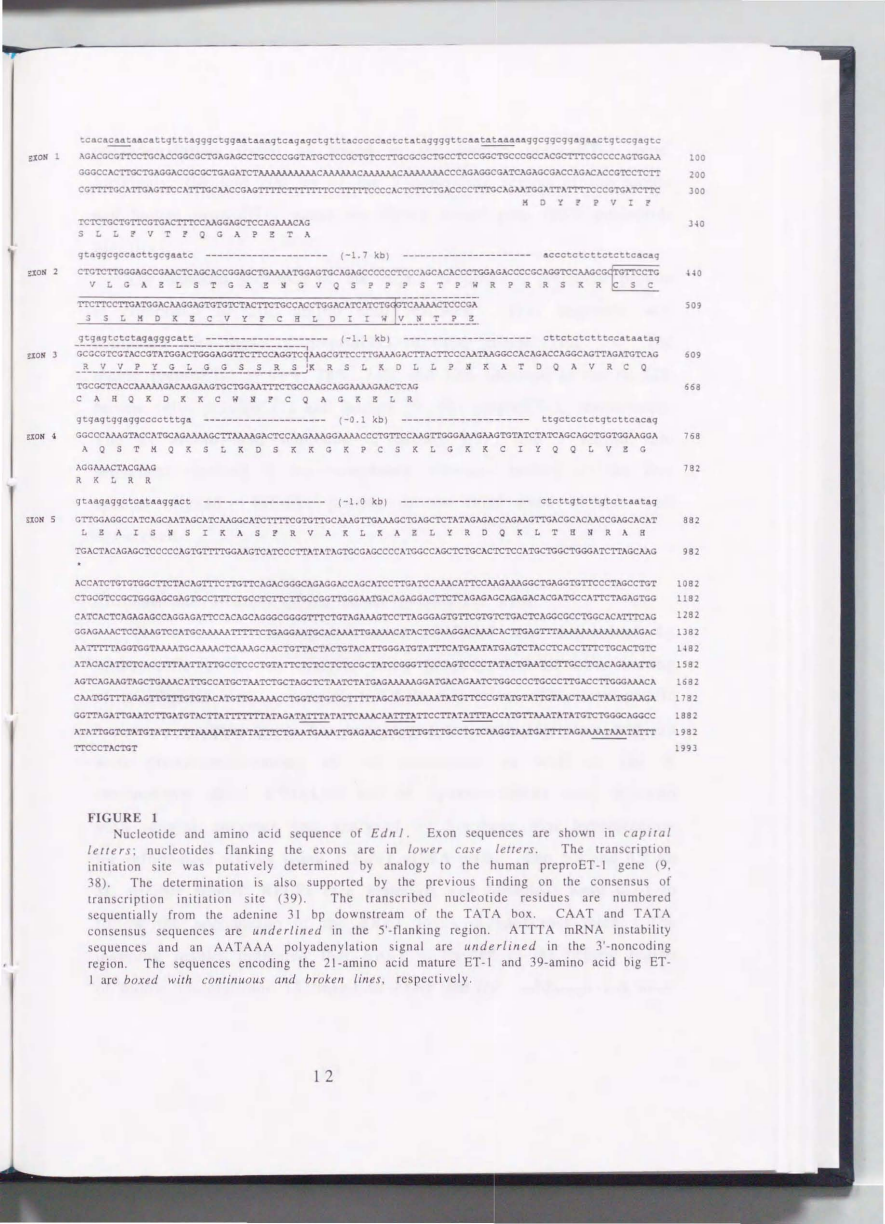

FIGURE 1

Nucleotide and amino acid sequence of *Edn1*. Exon sequences are shown in *capital letters*; nucleotides flanking the exons are in *lower case letters*. The transcription initiation site was putatively determined by analogy to the human preproET-1 gene (9, 38). The determination is also supported by the previous finding on the consensus of transcription initiation site (39). The transcribed nucleotide residues are numbered sequentially from the adenine 31 bp downstream of the TATA box. CAAT and TATA consensus sequences are *underlined* in the 5'-flanking region. ATTTA mRNA instability sequences and an AATAAA polyadenylation signal are *underlined* in the 3'-noncoding region. The sequences encoding the 21-amino acid mature ET-1 and 39-amino acid big ET-1 are *boxed with continuous and broken lines*, respectively.

polyadenylation signal as found in the human preproET-1 gene. Strikingly, the last 200 bp of the 3'-noncoding region of the mouse and human preproET-1 genes are highly homologous (93% nucleotide identity).

The deduced sequence of the mouse preproET-1 precursor protein is composed of 202 amino acid residues. This sequence was compared with those of preproET-1 of other species (Fig. 2). The mouse preproET-1 is 91%, 78%, 74% and 70% identical to the rat (25, bovine (40), porcine (1) and human (9, 38) preproET-1, respectively. The 21 amino acid sequence of mature ET-1 and 5 amino acid sequences flanking it are completely identical among all the five species aligned. ET-like peptide in the third exon is also well conserved.

Chromosomal location of the mouse preproET-1 gene

The mouse chromosomal location of *Edn1* was determined by interspecific backcross analysis using progeny derived from mating of [(C57BL/6J × *M. spretus*)F_1 × C57BL/6J] mice. This interspecific backcross mapping panel has been typed for over 1800 loci that are well distributed among all the autosomes as well as the X chromosome (26). C57BL/6J and *M. spretus* DNAs were digested with several enzymes and analyzed by Southern blot hybridization for informative RFLPs using a *Edn1* cDNA probe. The 5.8 and 4.7 kb *M. spretus* *Hin*dIII RFLPs (see Materials and Methods) were used to follow the segregation of the *Edn1* locus in backcross mice. The mapping results indicated that *Edn1* is located in the central region of mouse chromosome 13 linked to *Fim1* and *Il9*. Although 164 mice

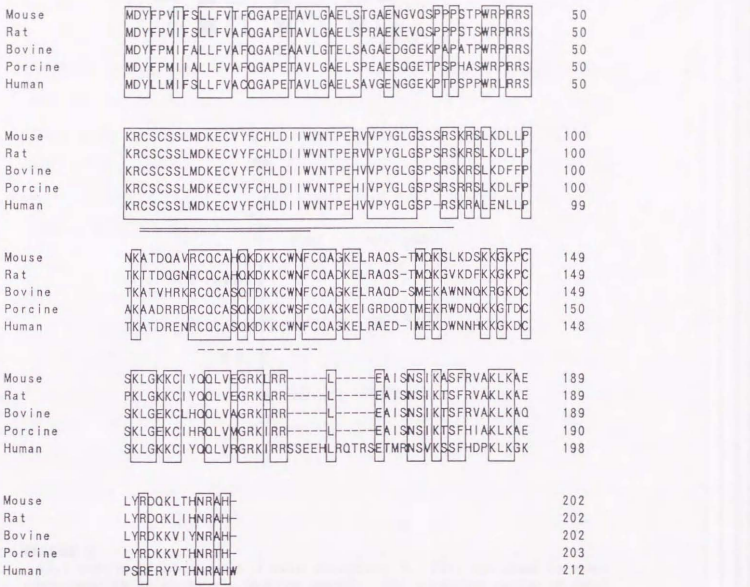

FIGURE 2

Alignment of the amino acid sequences of mouse, rat , bovine , porcine and human preproET-1. Amino acid residues identical among all the species are boxed. Mature ET-1 is *doubly underlined* and big ET-1 is *singly underlined*. ET-like peptide is *underlined with broken line*.

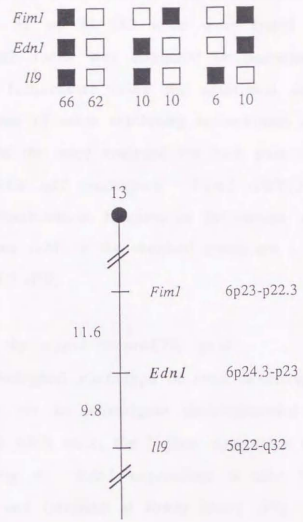

FIGURE 3

Edn1 maps in the central region of mouse chromosome 13. *Edn1* was placed on mouse chromosomal 13 by interspecific backcross analysis. The segregation patterns of *Edn1* and flanking genes in 164 backcross animals that were typed for all loci are shown at the top of the figure. For individual pairs of loci, more than 164 animals were typed (see text). Each column represents the chromosome identified in the backcross progeny that was inherited from the (C57BL/6J × *M. spretus*)F_1 parent. The shaded boxes represent the presence of *M. spretus* allele. The number of offspring inheriting each type of chromosome is listed at the bottom of each column. A partial chromosome 13 linkage map showing the location of *Edn1* in relation to linked genes is shown at the bottom of the figure. Recombination distances between loci in centimorgans are shown to the left of the chromosome and the position of loci in human chromosomes, where known, are shown to the right. References for the human map positions of loci cited in this study can be obtained from GDB (Genome Data Base), a computerized database of human linkage information maintained by The William H. Welch Medical Library of The Johns Hopkins University (Baltimore, MD).

were analyzed for every marker and are shown in the segregation analysis (Fig. 3), up to 183 mice were typed for some pairs of markers. Each locus was analyzed in pairwise combinations for recombination frequencies using the additional data. The ratios of the total number of mice exhibiting recombinant chromosomes to the total number of the mice analyzed for each pair of loci and the most likely gene order are: centromere - *Fim1* -20/173 - *Edn1* - 18/183 - *Il9*. The recombination frequencies [expressed as genetic distances in centiMorgans (cM) ± the standard error] are - *Fim1* - 11.6 ± 2.4 - *Edn1* - 9.8 ± 2.2 -*Il9*.

Expression of the mouse preproET-1 gene

The morphological phenotype of mice homozygous for *Edn1* null allele aroused me to investigate developmental changes in *Edn1* expression. In adult mice, the highest expression of *Edn1* is detected in the lung (Fig. 4). *Edn1* expression is also found in the heart, kidney, brain and intestine at lower levels (Fig. 4). These patterns are similar to those previously reported in other species (25).

Temporal profiles of *Edn1* expression were examined and compared with those of *Edn3* in the mouse lung, which is the most abundant site of ET-1 expression among adult mice tissues. In 17.5 d.p.c. fetal mice, *Edn1* expression is relatively low in the lung and the expression level increases as the animal grows (Fig. 5A). In contrast, the expression of *Edn3* is markedly decreased during the perinatal stage (Fig. 5B). The peptide levels of ET-1 and ET-3 are in parallel with the mRNA levels of *Edn1* and *Edn3* (Fig. 6). The levels of ET-3 are about one-third of those of ET-1 in the fetal lung.

FIGURE 4

Northern blot analysis of *Edn1* mRNA in adult mouse tissues. Total RNA samples were prepared from the heart (*lane 1*), lung (*lane 2*), kidney (*lane 3*), brain (*lane 4*), and intestine (*lane 5*) of 8-week old male ICR mice. Thirty μg of RNA per lane was electrophoresed, blotted onto nylon membrane and hybridized to *Edn1* RNA probes. The positions of 28S and 18S rRNA and *Edn1* mRNA are indicated.

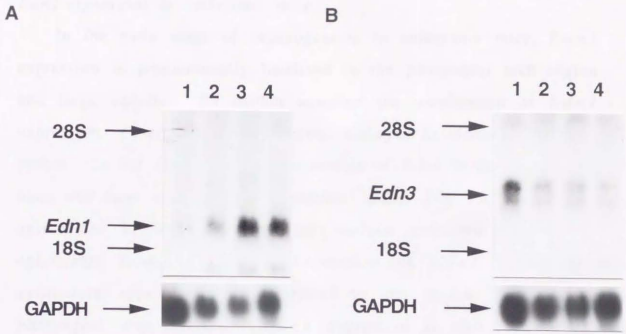

FIGURE 5

Northern blot analysis of *Edn1* (**A**) and *Edn3* (**B**) mRNA in the mouse lung at different developmental stages. Total RNA samples were prepared from the lung of 17 d.p.c. fetuses (*lane 1*), 0-day old neonates (*lane 2*), 6-week old adolescents (*lane 3*), and 30-week old adults (*lane 4*). Twenty μg (**A**) or thirty μg (**B**) of RNA per lane was electrophoresed, blotted onto nylon membrane and hybridized to *Edn1* or *Edn3* RNA probes. The positions of 28S and 18S rRNA and *Edn1* or *Edn3* mRNA are indicated.

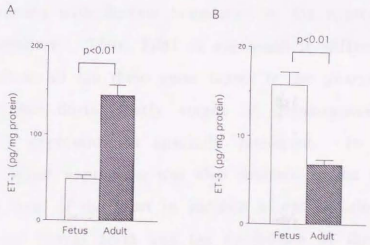

FIGURE 6

ELISA for ET-1 (**A**) and ET-3 (**B**) in the mouse lung at different developmental stages. The contents of ET-1 and ET-3 were compared between 17 d.p.c. fetuses (**A**, n=8; **B**, n=17) and 8-10-week old adult mice (**A**, n=7; **B**, n=11).

Edn1 expression in embryonic mice.

In the early stage of organogenesis in embryonic mice, *Edn1* expression is predominantly localized in the pharyngeal arch region and large vessels. To further examine the localization of *Edn1* expression, I sectioned whole-mount embryos hybridized to *Edn1* probes. In 9.0 d.p.c. embryos, expression of *Edn1* is detected in the outer and inner surface of the pharyngeal arches (Fig. 7A). The outer epithelium is derived from the surface ectoderm; the inner epithelium from endoderm. Expression of *Edn1* in the outer epithelium appears to be restricted to the medial half of the pharyngeal arch surface. *Edn1* expression is also seen in the pharyngeal mesenchyme, which is mainly composed of neural crest-derived ectomesenchymal cells (Fig. 7A). The endothelium of the dorsal aorta and arch arteries, whose origin is paraxial and lateral mesoderm, also expresses *Edn1* (Fig 7A). In sagittal sections, the epithelium of the pharyngeal pouches gives high expression of *Edn1* (Fig. 7B). *Edn1* expression in the pharyngeal pouch epithelium shows a restrictive pattern with distinct boundaries as the expression in the outer arch epithelium. Thus, Edn1 is expressed in different types of cells derived from all the three germ layers in the pharyngeal region and large arteries during early stages of organogenesis and the pattern of this expression is spacially restricted. In 10.0 d.p.c. embryos, high *Edn1* expression was also detected in the endocardium of the outflow tract of the heart in addition to the endothelium of the arch arteries and dorsal aorta and the epithelium of the pharyngeal arches (Fig. 8A, B). In the heart of 11.5 d.p.c. embryos, ET-1 signal was apparent in the conotruncal region in a spiral pattern (Fig. 8C).

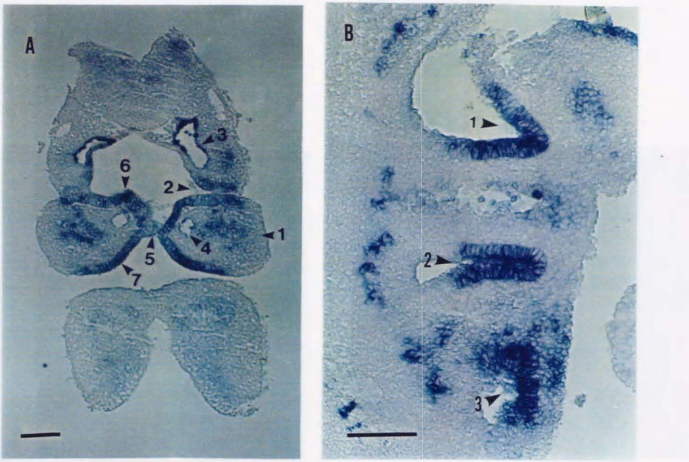

FIGURE 7

In situ hybridization of 9.0 d.p.c. mouse embryos with *Edn1* probe. (**A**) Transverse section at the level of the first pharyngeal arch. 1, first pharyngeal arch; 2, first pharyngeal pouch; 3, dorsal aorta; 4, first pharyngeal artery; 5, buccopharyngeal membrane; 6, endoderm-derived epithelium; 7, ectoderm-derived epithelium. (**B**) Sagittal section of the pharyngeal arches. 1, 2 and 3; first, second and third pharyngeal pouches, respectively. *Edn1* expression is detected in the endoderm- and ectoderm-derived epithelium and mesenchyme of the pharyngeal arches and pouches, and the endothelium of the large arteries. Bar, 0.1mm.

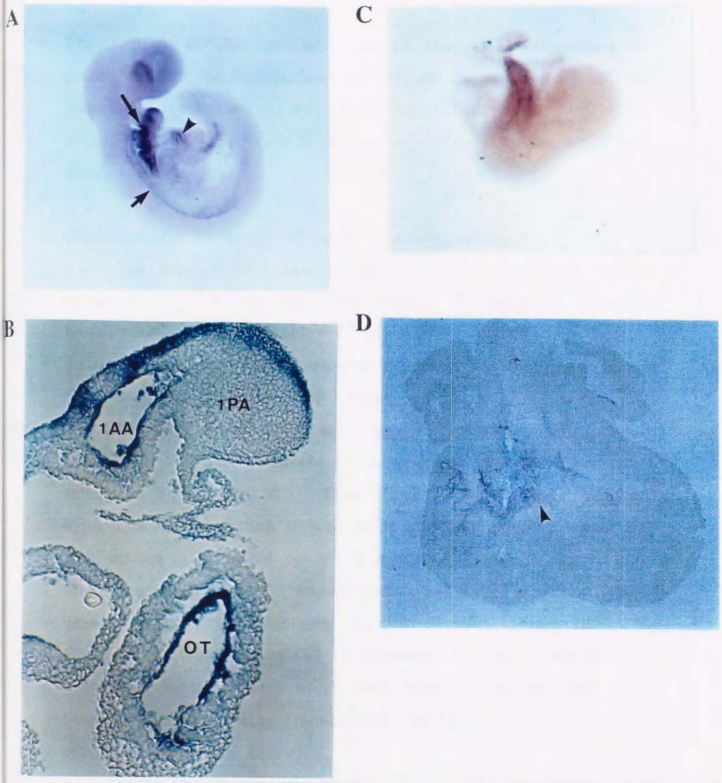

FIGURE 8

In situ hybridization of mouse embryos with the ET-1 probes. (**A**) Whole-mount hybridization of 10.0 d.p.c. embryo. Arrowhead indicates ET-1 signal in the outflow tract of the heart; long arrow, ET-1 signal in the epithelium of the pharyngeal arches; short arrow, ET-1 signal along the dorsal aorta. (**B**) Paraffin section of **A**. ET-1 expression is detected in the endocardium of the outflow tract (OT), the endothelium of the first pharyngeal arch artery (1AA) and the epithelium of the first pharyngeal arch (1PA). (**C**) Whole-mount hybridization of the heart dissected from 11.5 d.p.c. embryo. High ET-1 expression is detected in the conotruncal region (arrowhead). (**D**) Paraffin section of **C**. ET-1 expression is predominantly detected in the endocardial cushion (arrowhead).

The section of the specimen showed that ET-1 expression is predominant in the endocardium as well as the mesenchyme of the endocardial cushion at this stage (Fig. 8D). These results support the notion that ET-1 is involved in the development of the heart and great vessels.

Cardiovascular phenotype of Edn1$^{-/-}$ homozygous mice.

The role of ET-1 in cardiovascular development was further examined by analyzing the cardiovascular phenotype of *Edn1*$^{-/-}$ homozygous mice. Table 1 summarizes the cardiovascular malformations of *Edn1*$^{-/-}$ homozygous fetuses at 18.5 d.p.c.. Some *Edn1*$^{-/-}$ homozygotes displayed tubular hypoplasia of the aortic arch (Fig. 9B), interruption of the aorta distal to the left common carotid artery (Fig. 9C) and/or absence of the proximal segment of the right subclavian artery (Fig. 9C). Even *Edn1*$^{-/-}$ homozygotes without hypoplasia or interruption showed aortic arch deformity in which the arch seemed to be pulled upward in a manner similar to that in Fig. 9B. In most of *Edn1*$^{-/-}$ homozygotes, additional small arteries branched from the common carotid arteries (Fig. 9B, C). Furthermore, many of *Edn1*$^{-/-}$ homozygotes also showed tiny ventricular septal defect, which was increased in size and well characterized by using monoclonal antibodies or a receptor antagonist (described below).

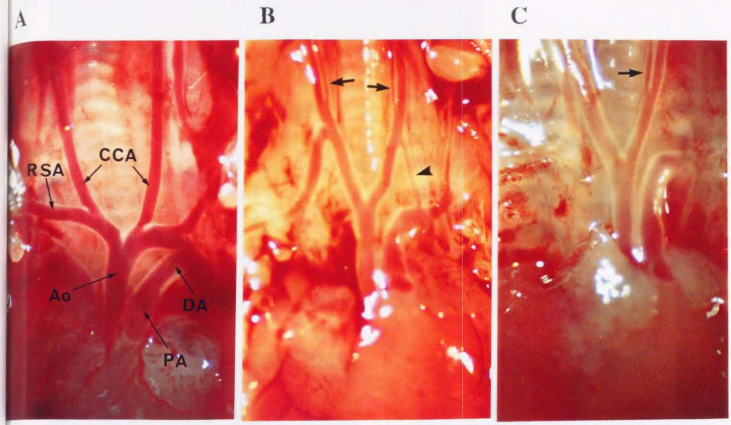

FIGURE 9

Typical patterns of cardiovascular abnormalities in *Edn1*$^{-/-}$ homozygous mice at 18.5 d.p.c.. Normal control hearts and great vessels of *Edn1*$^{+/+}$ wild type fetuses (**A** and **D**) and those of monoclonal antibodies-treated *Edn1*$^{-/-}$ homozygous fetuses (**B** through **F**) were presented. (**A**) Normal heart and great vessels of a wild-type fetus. Ao, aorta; PA, pulmonary artery; DA, ductus arteriosus; CCA, common carotid arteries; RSA, right subclavian artery. (**B**) Deformed aortic arch with tubular hypoplasia (arrowhead) of an *Edn1*$^{-/-}$ homozygote. Arrows indicate extra arteries branching from the common carotid arteries. (**C**) Aortic arch interruption and absent right subclavian artery of an *Edn1*$^{-/-}$ homozygote. Extra arteries are also seen (an arrow). (**D**) Appearance of a normal heart (*left*) and an *Edn1*$^{-/-}$ homozygous heart (*right*). The right ventricle is enlarged (arrow) in the *Edn1*$^{-/-}$ homozygote. (**E**) Ventricular septal defect of an *Edn1*$^{-/-}$ homozygote. The defect (arrowhead) appears to be perimembranous and located in the outlet of the ventricle. The aorta overrides the crest of the ventricular septum. Ao, aorta; Inf, infundibulum; ST, septomarginal trabeculation of the right ventricle. (**F**) Haematoxylin-eosin-stained histological section of an *Edn1*$^{-/-}$ homozygous heart showing ventricular septal defect (arrowhead) and overriding aorta. LV, left ventricle; RV, right ventricle; Ao, Aorta.

D

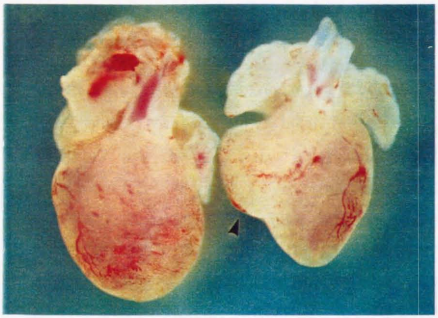

E

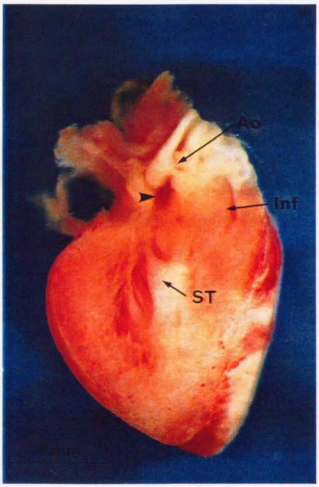

F

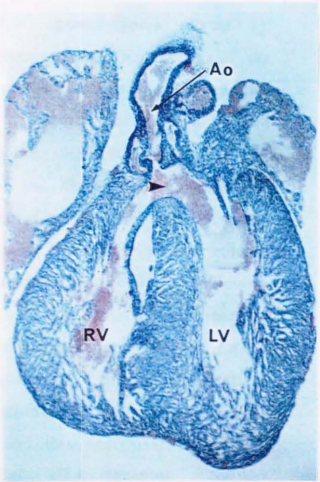

FIGURE 9 (Continued)

Effects of anti-ET-1-monoclonal antibodies and ET antagonist on the cardiovascular phenotype.

Because these cardiovascular malformations appeared in *Edn1*$^{-/-}$ homozygotes with incomplete penetration, I hypothesized that ET-1 function may be partially compensated by maternally-derived circulating ET-1 or other ET isoforms, ET-2 and ET-3. To test this hypothesis, I implanted osmotic minipumps containing neutralizing monoclonal antibodies specific for ETs or an ET_A-receptor-selective antagonist, BQ123, in pregnant *Edn1*$^{+/-}$ heterozygotes and examined the phenotype of the offspring. Continuous administration of monoclonal antibodies or BQ123 resulted in increased occurrence of aortic arch malformations in *Edn1*$^{-/-}$ homozygotes (Table 1). Ventricular septal defect was encountered more frequently and the defect size tended to be larger than untreated *Edn1*$^{-/-}$ homozygotes (Table 1). The ventricular septal defect is perimembranous and located beneath the outflow tract supporting the aortic valve (Fig. 9E, F). The aorta frequently overrided the crest of the ventricular septum or arisen mainly from the right ventricle (Fig. 9E, F). The right ventricles were typically dilated, which indicates volume overload probably due to left-to-right shunt (Fig. 9D). Continuous infusion of saline or control monoclonal antibodies did not increase the frequency or extent of the cardiovascular abnormalities of *Edn1*$^{-/-}$ mice (data not shown). These results suggest that circulating ET-1 and/or other ET isoforms may compensate the role of endogenous ET-1 in cardiovascular development and this functional redundancy may be mediated by, at least in part, ET_A receptor. Neither cardiovascular nor craniofacial abnormalities were found in *Edn1*$^{+/-}$

heterozygous or *Edn1*$^{+/+}$ wild-type littermates in any condition, suggesting that neither neutralizing antibodies nor BQ123 at the doses used are sufficient to abolish the role of endogenous ET-1 in embryogenesis.

TABLE 1 Cardiovascular abnormalities in *Edn1*$^{-/-}$ homozygous mice

	Untreated (%)	MAb-treated (%)	BQ123-treated (%)
Abnormalities of the great vessels			
Tubular hypoplasia of the aorta	2 / 43 (4.6)	11 / 55 (20.0) *	7 / 34 (20.6) *
Interruption of the aorta	1 / 43 (2.3)	8 / 55 (14.5) *	8 / 34 (23.5) **
Absent right subclavian artery	4 / 31 (12.9)	11 / 43 (25.6)	13 / 21 (61.9) **
Ventriclar septal defect	15 / 31 (48.4)	29 / 35 (82.9) **	17 / 19 (89.5) **

*P<0.05, **P<0.01 versus the control untreated group.

Developmental patterns of the pharyngeal arch arteries.

To clarify the genesis of these cardiovascular abnormalities in *Edn1*$^{-/-}$ homozygotes, I compared the developmental patterns of the pharyngeal arch arteries and heart at the stage of organogenesis. In normal embryos, the first and second arch arteries disappear before 11 d.p.c. and the left fourth arch artery well develops to generate the isthmus of the aortic arch together with the dorsal aorta. Both third arch arteries and right fourth artery give rise to the common carotid arteries and the proximal region of the right subclavian artery,

respectively (41 and Fig. 10A, B). In *Edn1*$^{-/-}$ homozygous embryos, the first or second arch artery persisted, possibly corresponding to the extra arteries branching from the carotid arteries at 18.5 d.p.c., and both fourth arch arteries were diminished (Fig. 10A, B). Instead, a communication between the left third arch artery and dorsal aorta seemed to form the deformed aorta. The occurrence of aortic tubular hypoplasia or interruption seemed to be dependent on the development of the dorsal aorta between the third arch artery and ductus arteriosus (the sixth arch artery). Thus, alterations in the pattern of arch artery development lead to the aortic arch abnormalities in *Edn1*$^{-/-}$ homozygotes. In the heart of *Edn1*$^{-/-}$ homozygotes, endocardial cushion at the site of septation was poorly developed without fusing to the muscular septum (Fig. 10C, D). In some of BQ123-treated embryos, cell proliferation in the compact zone of the ventricular wall is poor (Fig. 10E).

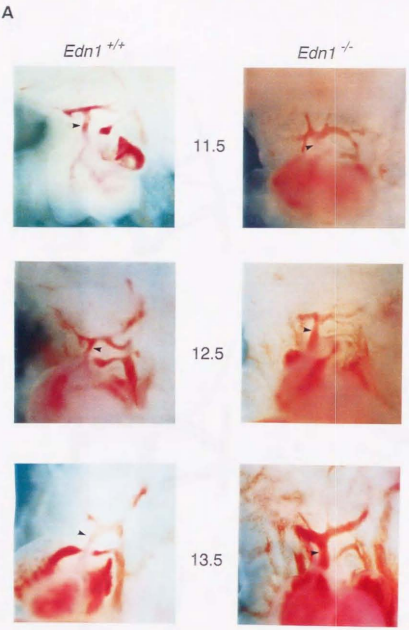

FIGURE 10

Development of the cardiovascular system in *Edn1*$^{+/+}$ wild-type and *Edn1*$^{-/-}$ homozygous mice. (**A** and **B**) Photographs and schematic drawings of the arch arteries at 11.5, 12.5 and 13.5 d.p.c. in *Edn1*$^{+/+}$ wild-type and *Edn1*$^{-/-}$ homozygous mice. The first or second pharyngeal arch artery persists and the fourth arch artery is poorly developed in *Edn1*$^{-/-}$ homozygotes. Arrowheads indicate the ventral aorta. (**C** through **E**) Histological sections of the heart at 13.5 d.p.c. in an *Edn1*$^{+/+}$ wild-type mouse (**C**), a monoclonal antibodies-treated *Edn1*$^{-/-}$ homozygotes (**D**) and an *Edn1*$^{-/-}$ homozygotes treated with BQ123 (**E**). Development of the endocardial cushion (EC) is retarded and the ventricular septum (arrow) is defected in *Edn1*$^{-/-}$ homozygotes. In a BQ123-treated *Edn1*$^{-/-}$ homozygotes, hypoplasia of the compact zone of the ventricular wall (arrowhead) is also displayed.

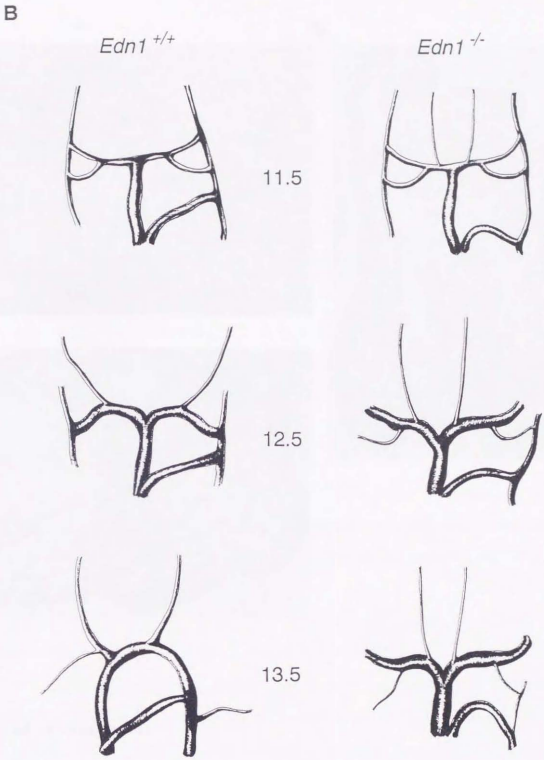

FIGURE 10 (Continued)

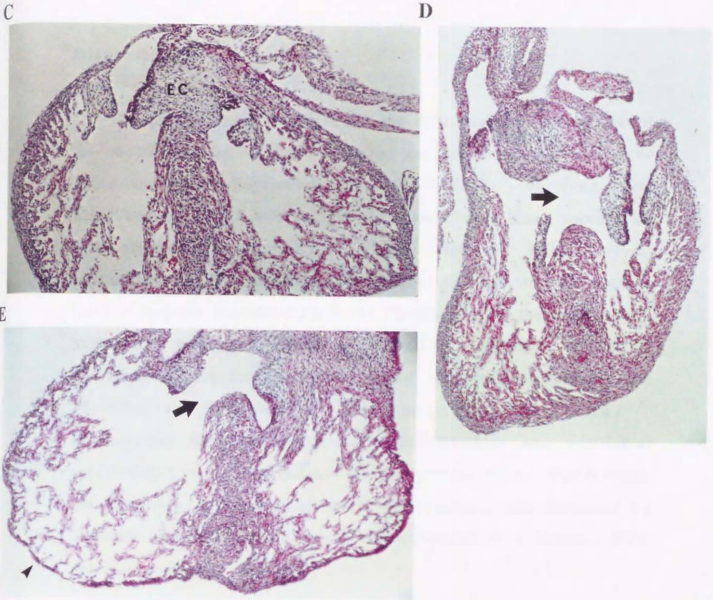

FIGURE 10 (Continued)

Discussion

The present study demonstrates the structural characterization of the mouse preproET-1 gene (*Edn1*), developmental expression of *Edn1* and the cardiovascular phenotype of *Edn1*$^{-/-}$ knockout mice. *Edn1* comprises of five exons and the open reading frame encodes for 202 amino acid preproET-1. The sequences and structural organization of *Edn1* are highly homologous to those of other species. *Edn1* expression was detected in the endothelium of the arch arteries and cardiac outflow tract and the endocardial cushion as well as in the epithelium of the pharyngeal arches, suggesting the involvement of ET-1 in cardiovascular development. In fact, *Edn1*$^{-/-}$ homozygotes displayed aortic arch malformations and ventricular septal defect with abnormalities of the outflow tract. Furthermore, the frequency and extent of these abnormalities were increased by treatment with neutralizing monoclonal antibodies or a selective ET_A receptor antagonist BQ123.

Characterization of the mouse preproET-1 gene

The sequences and structural organization of *Edn1* are highly homologous to those of other species, especially in the terminal 200 bp sequences of 3'-noncoding region. This terminal 200 bp sequences contains three ATTTA mRNA instability sequences as found in the human preproET-1 gene. Inoue *et al.* reported that human preproET-1 mRNA is an extremely labile molecule with an intracellular life span of approximately 15 min (9). These data suggest that the terminal 200 bp sequences of the 3'-noncoding

region is important for posttranscriptional regulation of *Edn1* mRNA metabolism.

The deduced sequence of the mouse preproET-1 precursor protein is composed of 202 amino acid residues. The 21 amino acid sequence of mature ET-1 and 5 amino acid sequences flanking it are completely identical among all the five species aligned. The C-terminal region of preproET-1 is rich in basic amino acids. Of 38 amino acid residues of the C-terminal region of mouse preproET-1, 11 residues are basic. Although this region is less homologous among species compared with other regions, 9 of 11 basic residues are identical among species, suggesting that this basic region may be functionally important.

Chromosomal location of the mouse preproET-1 gene

Interspecific backcross mapping located *Edn1* in the central region of chromosomal 13. Mice homozygous for ET-1 null mutation die around birth of respiratory failure and also display numerous craniofacial abnormalities (18). To determine whether there were any spontaneous mutations that mapped in the vicinity of *Edn1* and showed a phenotype similar to that of *Edn1* null mutants, I have compared the interspecific map of chromosome 13 with a composite mouse linkage map that reports the map location of many uncloned mouse mutations (compiled by M. T. Davisson, T. H. Roderick, A. L. Hillyard, and D. P. Doolittle and provided from GBASE, a computerized database maintained at The Jackson Laboratory, Bar Harbor, ME). *Edn1* mapped in a region of the composite map that contains one

mouse mutation with a phenotype similar to that seen with mice homozygous for a null allele of *Edn1* (data not shown).

This mutation is congenital hydrocephalus (*ch*). Mice homozygous for *ch* die around birth from an inability to breath. These animals also display a wide variety of skeletal and urogenital abnormalities (42). Because *ch* mice appear to have a more severe phenotype than *Edn1* knockout mice, *ch* may affect more genes than just the *Edn1* locus. Thus, it would be interesting to determine whether *ch* is allelic with the *Edn1* null mutation.

Developmental expression of Edn1 in mice.

In situ hybridization demonstrated that *Edn1* expression in the epithelium of the pharyngeal arches and pouches was restricted to specific regions with relatively distinct boundaries. This pattern of expression is reminiscent of the expression of homeobox genes (43). In early stages of organogenesis when *Edn1* expression is evident, various homeobox genes are expressed in the pharyngeal region and their expression is regulated in a spatial- and temporal-specific manner (44-48). Although there is no homeobox gene whose expression pattern is identical to that of *Edn1*, it would be of interest to examine possible interactions between *Edn1* and homeobox genes.

In the embryonic cardiovascular system, the intense expression of *Edn1* is detected in the endocardium of the conotruncal region in comparison to that of the atrioventricular region. The conotruncal region forms differently than the other segments of the primary heart tube. This region is not yet present at the stage of fusion of the epimyocardial troughs; rather it appears in subsequent stages of

development (49). Correspondingly, conotruncal endocardial cells do not share common precursors with atrioventricular endocardial cells. Precursor cells from cephalic paraxial and lateral mesoderm migrate into the outflow tract to form the conotruncal endocardium, whereas precursor cells of the atrioventricular endocardium are derived from the cardiogenic plates (50). Differences in the pattern of *Edn1* expression may be correlated to this developmental heterogeneity.

Comparison of changes in *Edn1* and *Edn3* gene expression levels at different developmental stages provided another important information about differential role of the two isoforms in development. *Edn1* expression and ET-1 peptide levels in the lung are progressively increased during the perinatal stage, whereas the expression of *Edn3*, a gene encoding ET-3, is reciprocally decreased. These results suggest that *Edn1* and *Edn3* expression is temporally and reciprocally regulated during perinatal development. Further investigation of the expression of the ET family may give a clue as to their role in development of different tissues and organs and possible redundancy of function among the isopeptides.

Cardiovascular phenotype of Edn1$^{-/-}$ homozygous mice.

In the present study, I have also demonstrated that *Edn1*$^{-/-}$ homozygous mice develop cardiovascular malformations involving the heart and great vessels with incomplete penetration. Treatment with neutralizing monoclonal antibodies specific for ET or ET_A receptor antagonist BQ123 significantly increased the frequency and extent of these cardiovascular abnormalities. The development of the pharyngeal arch arteries and endocardial cushion is affected in

Edn1$^{-/-}$ homozygotes. Furthermore, *Edn1* is expressed in the endothelium of the arch arteries and cardiac outflow tract and the endocardial cushion as well as in the epithelium of the pharyngeal arches at the stage of early organogenesis. These results indicate a novel role of ET-1 in the cardiovascular development through, at least partly, ET_A receptor.

We previously proposed that neural crest-derived ectomesenchymal cells may be the major target of ET-1 in the craniofacial development (18). In the cardiovascular development, neural crest-derived ectomesenchymal cells which migrate from the pharyngeal arches to the outflow tract and walls of the arch arteries participate in outflow septation and formation of the great vessels (21-23)(Fig. 11). These ectomesenchymal cells provide support for the endothelium of the aortic arch arteries and form smooth muscle of the tunica media. Kirby et al. have shown that ablation of the neural crest results in outflow septation defects and aortic arch abnormalities similar to those of *Edn1*$^{-/-}$ homozygotes in the chick embryo (51, 52). Particularly, neural crest ablation causes disproportionate development of the third, fourth and sixth arch arteries which form the proximal part of the great arteries, resulting in aortic arch malformations including aortic arch interruption. The developmental pattern of the arch arteries in *Edn1*$^{-/-}$ homozygotes also represented similar inappropriate formation of the arch arteries and are consistent with disturbance in neural crest-derived cell lineage. In the process of aortic arch formation, interactions among all the elements of the pharyngeal arches including vascular endothelium, endoderm-derived epithelium of the pharyngeal pouch,

ectoderm-derived epithelium of the pharyngeal grooves and arches, and neural crest-derived ectomesenchyme determine the fate of each arch arteries (21, 22). In my present study, phenotypic manifestations of *Edn1*$^{-/-}$ homozygotes and high expression of ET-1 in the vascular endothelium and pharyngeal arch epithelium suggest that ET-1 may participate in these interactions as a factor from vascular endothelium and pharyngeal epithelium to determine the arch artery development and that the cardiac neural crest cell lineage may be the major target of ET-1 in cardiovascular development.

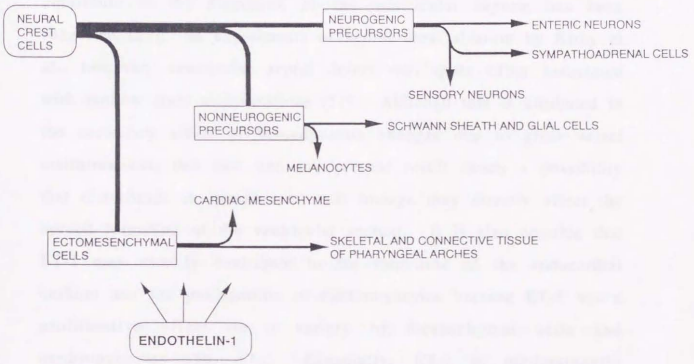

FIGURE 11
Segregation of neural crest sublineages and possible involvement of endothelin-1

The genesis of ventricular septal defect is rather complicated. In the ventricular wall, the condense trabeculae at the interventricular groove give rise to the rudiment of the septum and grow inward, forming the major muscular portion of the septum (53). On the other hand, the endocardial cushion is formed by mesenchymal cells derived from endocardial cells migrating through a specialized extracellular matrix, cardiac jelly (54, 55). The endocardial cushion further expands to fuse with the muscular ventricular septum and aorticopulmonary septum, forming the membranous portion of the ventricular septum. Neural crest-derived cells have not been detected in this area and no direct evidence that neural crest cells contribute to the formation of the ventricular septum has been suggested (21). In experiments of neural crest ablation by Kirby et al., however, ventricular septal defect was quite often associated with outflow tract malformations (51). Although this is attributed to the secondary effect of hemodynamic changes due to great vessel malformations, this fact and my present result raises a possibility that disturbance in neural crest cell lineage may directly affect the normal formation of the ventricular septum. It is also possible that ET-1 may directly contribute to the formation of the endocardial cushion and the proliferation of cardiomyocytes because ET-1 has a proliferative effect on a variety of mesenchymal cells and cardiomyocytes (56, 57). Especially, ET-1 is predominantly expressed in the endocardial cushion at 11.5 d.p.c., when the cushion is soon to form the membranous component of the interventricular septum. It requires further investigation to determine the target cells of ET-1 effects in the ventricular septal formation.

This study also indicates the existence of functional redundancy in the ET system in the cardiovascular development. It cannot be definitely determined whether the functional redundancy of the role of ET-1 in cardiovascular development is caused by maternally derived circulating ET-1 or other ET isoforms (ET-2 and/or ET-3). However, the following evidence argues against the latter possibility; i) ET-2 is not detected in circulating blood and the plasma level of ET-3 is less than that of ET-1 (31, 58). ii) The affinity of ET-3 to ET_A receptor is about a thousand times as low as that of ET-1 and ET-2 (59). iii) Neither ET-2 nor ET-3 mRNA is detected in the heart of wild-type and homozygous mice (my unpublished data). Taken together, I am inclined to suppose that maternally derived ET-1 could cause partial rescue of the cardiovascular phenotype of ET-1 null mutation. Recently, TGF-β1 null mutation is reported to be rescued by maternal TGF-β1 (60). The present result may be another example of maternal rescue of targeted gene disruption of secreted proteins.

Clinical implications

In human diseases, ventricular septal defect and aortic arch anomalies including type B aortic arch interruption are shown to be associated with or be a part of congenital syndromes including Pierre-Robin syndrome (61), DiGeorge syndrome (62, 63) and velo-cardio-facial syndrome (64), which involves craniofacial tissues and organs. The manifestations of these syndromes are quite similar to the phenotype of *Edn1*$^{-/-}$ homozygotes. Many cases of these syndromes are closely linked to deletions in chromosome 22q11 (62-

64). Although the human ET-1 gene maps to chromosome 6 (27), this similarity of phenotype argues for a common developmental feature. Recently a candidate gene, DGCR3, involved in the etiology of DiGeorge syndrome has been identified (65). Although the function of the gene product remains unknown, the predicted protein disrupted by the t(2; 22) contains a leucine zipper motif, suggesting that the candidate gene may be a DNA binding protein. Thus ET-1 and DGCR3 product may be involved in the molecular network in the craniofacial development. In this context, the *Edn1*$^{-/-}$ homozygous mice may be a useful model for these syndromes.

Recently, several genes have been suggested as contributors in cardiogenesis by transgenic approaches (48, 53, 60, 66, 67). ET-1 may also participate in the molecular network in the cardiovascular development. Thus, investigations on ET-1 in relation to other factors will give a clue as to the clarification of the mechanism of the cardiovascular development and the pathogenesis of congenital heart diseases.

Conclusion

Taken all the present results together, I conclude that ET-1 is involved in the normal development of the heart and great vessels as well as the pharyngeal-arch-derived craniofacial tissues Especially, ET-1 knockout mice may serve as a good model for human congenital heart diseases.

References

1. Yanagisawa, M., H. Kurihara, S. Kimura, Y. Tomobe, M. Kobayashi, Y. Mitsui, Y. Yazaki, K. Goto, and T. Masaki. 1988. A novel vasoconstrictor peptide produced by vascular endothelial cells. *Nature* 332:411-415.
2. Inoue, A., M. Yanagisawa, S. Kimura, Y. Kasuya, T. Miyauchi, K. Goto, and T. Masaki. 1989. The human endothelin family: Three structurally and pharmacologically distinct isopeptides predicted by three separate genes. *Proc. Natl. Acad. Sci. USA.* 86:2863-2867.
3. Arai, H., S. Hori, I. Aramori, H. Ohkubo, and S. Nakanishi. 1990. Cloning and expression of a cDNA encording an endothelin receptor. *Nature* 348:730-732.
4. Sakurai, T., M. Yanagisawa, Y. Takuwa, H. Miyazaki, S. Kimura, K. Goto, and T. Masaki. 1990. Cloning of cDNA encoding a nonisopeptide-selective subtype of the endothelin receptor. *Nature* 348:732-735.
5. Takahashi, M., Y. Matsushita, Y. Iijima, and K. Tanzawa. 1993. Purification and characterization of endothelin-converting enzyme. *J. Biol. Chem.* 268:21395-21398.
6. Yoshizumi, M., H. Kurihara, T. Morita, T. Yamashita, Y. Oh-hashi, T. Sugiyama, F. Takaku, M. Yanagisawa, T. Masaki, and Y. Yazaki. 1990. Interleukin-1 induces the production of endothelin-1 by cultured endothelial cells. *Biochem. Biophys. Res. Commun.* 166:324-329.
7. Kurihara, H., M. Yoshizumi, T. Sugiyama, F. Takaku, M. Yanagisawa, T. Masaki, M. Hamaoki, H. Kato, and Y. Yazaki. 1989.

Transforming growth factor-beta stimulates the expression of endothelin mRNA by vascular endothelial cells. *Biochem. Biophys. Res. Commun.* 359:1435-1440.

8. Oliver, F.J., G. de la Rubia, E.P. Feener, M.E. Lee, M.H. Loeken, T. Shiba, T. Quertermous, and G.L. King. 1991. Stimulation of endothelin-1 gene expression by insulin in endothelial cells. *J. Biol. Chem.* 266:23251-23256
9. Inoue, A., M. Yanagisawa, Y. Takuwa, Y. Mitsui, M. Kobayashi, and T. Masaki. 1989. The human preproendothelin-1 gene. *J. Biol. Chem.* 264: 14954-14959
10. Yoshizumi, M., H. Kurihara, T. Sugiyama, F. Takaku, M. Yanagisawa, T. Masaki, and Y. Yazaki. 1989. Hemodynamic shear stress stimulates endothelin production by cultured endothelial cells. *Biochem. Biophys. Res. Commun.* 161:859-864
11. Morita, T., H. Kurihara, K. Maemura, M. Yoshizumi, and Y. Yazaki. 1993. Disruption of cytoskeletal structures mediates shear stress-induced endothelin-1 gene expression in cultured porcine aortic endothelial cells. *J. Clin. Invest.* 92:1706-1712
12. Lee, M.-E., K.D. Bloch, J.A. Clifford, and T. Quertermous. 1990. Functional analysis of the endothelin-1 gene promoter. *J. Biol. Chem.* 265:10446-10450
13. Ransone, L.J., and I.M. Verma. 1990. Nuclear proto-oncogenes fos and jun. *Annu. Rev. Cell. Biol.* 6: 539-557
14. Yanagisawa, M., and T. Masaki. 1989. Molecular biology and biochemistry of the endothelins. *Trends. Pharmacol. Sci.* 10:374-378.

15. Lüscher, T.F., C.M. Boulanger, Y. Dohi, and Z.H. Yang. 1992. Endothelium-derived contracting factors. *Hypertension* 19:117-130.

16. Masaki, T., S. Kimura, M.Yanagisawa, and K. Goto. 1991. Molecular and cellular mechanism of endothelin regulation. Implications for vascular function. *Circulation* 84:1457-1468.

17. Vanhoutte, P.M. 1994. A matter of life and breath. *Nature* 368: 693-694.

18. Kurihara, Y., H. Kurihara, H. Suzuki, T. Kodama, K. Maemura, R. Nagai, H. Oda, T. Kuwaki, W. H. Cao, N. Kamada, K. Jishage, Y. Ouchi, S. Azuma, Y. Toyoda, T. Ishikawa, M. Kumada, and Y. Yazaki. 1994. Elevated blood pressure and craniofacial abnormalities in mice deficient in endothelin-1. *Nature* 368:703-710.

19. Noden, D.M. 1991. Cell movements and control of patterned tissue assembly during craniofacial development. *J. Craniofac. Genet. Dev. Biol.* 11:192-213.

20. Vainio, S., I. Karavanova, A. Jowett, and I. Thesleff. 1993. Identification of BMP-4 as a signal mediating secondary induction between epithelial and mesenchymal tissues during early tooth development. *Cell* 75:45-58.

21. Kirby, N.L., and K.L. Waldo. 1990. Role of neural crest in congenital heart disease. *Circulation* 82:332-340.

22. Kirby, M.L. 1993. Cellular and molecular contributions of the cardiac neural crest to cardiovascular development. *Trends. Cardiovasc. Med.* 3:18-23.

23. Fishman, M.C., and D.Y. Steinier. 1994. Cardiovascular development. Prospects for a genetic approach. *Circ. Res.* 74:757-763.

24. Saida, K., Y. Mitsui, and N. Ishida. 1989. A novel peptide, vasoactive intestinal contractor, of a new(endothelin) peptide family. *J. Biol. Chem.* 264: 14613-14616

25. Sakurai, T., M. Yanagisawa, A Inoue, U.S. Ryan, S. Kimura, Y. Mitsui, K. Goto, and T. Masaki. 1991. cDNA cloning, sequence analysis and tissue distribution of rat preproendothelin-1 mRNA. *Biochem. Biophys. Res. Commun.* 175: 44-47

26. Copeland, N.G., and N.A. Jenkins. 1991. Development and applications of a molecular genetic linkage map of the mouse genome. *Trends. Genet.* 7: 113-118

27. Jenkins, N.A., N.G. Copeland, B.A. Taylor, and B.K. Lee. 1982. Organization, distribution, and stability of endogenous ecotropic murine leukemia virus DNA sequences in chromosomes of Mus musculus. *J. Virol.* 43: 26-36

28. Wilkie, T.M., Y. Chen, D.J. Gilbert, K.J. Moore, L. Yu, M.I. Simon, N.G. Copeland, and N.A. Jenkins. 1993. Identification, chromosomal location, and genome organization of mammalian G-protein-coupled receptors. *Genomics* 18: 175-184

29. Green, E.L. 1981 *In* "Genetics and probability in animal breeding experiments ", pp.77-113, Oxford University Press, New York

30. Yanagisawa, M., A. Inoue, T. Ishikawa, Y. Kasuya, S. Kimura, S. Kumagaye, K. Nakajima, T.X. Watanabe, S. Sakakibara, K. Goto, and T. Masaki. 1988. Primary structure, synthesis, and biological activity of rat endothelin, an endothelium-derived

vasoconstrictor peptide. *Proc. Natl. Acad. Sci. U. S. A.* 85: 6964-6967

31. Suzuki, N., H. Matsumoto, C. Kitada, T. Masaki,and M. Fujino. 1989. A sensitive sandwich-enzyme immunoassay for human endothelin. *J. Immunol. Methods.* 118:245-250.
32. Imokawa, G., Y. Yada, and M. Miyagishi. 1992. Endothelins secreted from human keratinocytes are intrinsic mitogens for human melanocytes. *J. Biol. Chem.* 266: 18352-18357
33. Wilkinson, D. 1992. Whole mount in situ hybridization of vertebrate embryos. *In In situ* hybridization: a practical approach. D. Wilkinson, editor. IRL, Oxford. 75-84.
34. Hamaoki, M., H. Kato, M. Sugi, M. Fujimoto, H. Kurihara, M. Yoshizumi, M. Yanagisawa, S. Kimura, T. Masaki, and Y. Yazaki. 1990. Monoclonal antibodies to endothelin: application for sandwich immunoassays. *Hybrydoma* 9:63-69.
35. Ihara, M., K. Noguchi, T. Saeki, T. Fukuroda, S. Tuchida, S. Kimura, T. Fukami, K. Ishikawa, M. Nishikibe, and M. Yano. 1992. Biological profiles of highly potent novel endothelin antagonists selective for the ETA receptor. *Life Sci.* 50:247-255.
36. Miyauchi, T., R. Yorikane, S. Sasaki, T. Sakurai, M. Okada, M. Nishikibe, M. Yano, I. Yamaguchi, Y. Sugishita, and K. Goto. 1993. Contribution of endogenous endothelin-1 to the progression of cardiopulmonary alternations in rats with monocrotaline-induced pulmonary hypertension. *Circ. Res.* 73:887-897.
37. Anderson, R.H., A.E. Becker, and W.B. Robertson. 1993. Systemic Pathology Volume 10. The Cardiovascular System. R.B. Robertson editor. Churchill Livingstone, Edinburgh.

38. Bloch, K.D., S.P. Friendrich, Mu-En Lee, R.L. Eddy, T.B. Shows, and T. Quertermous. 1989. Structural organization and chromosomal assignment of the gene encording endothelin. *J. Biol. Chem.* 264:10851-10857.

39. Lewin, B. 1994. Control at initiation: RNA polymerase-promoter interactions. In "Genes V", pp377-412, Oxford University Press, New York

40. Elshourbagy, N., P. Kmetz and G.M. Sathe. 1990. Nucleotide sequence of endothelin cDNA from bovine endothelial cells. *Nucleic Acid Res.* 18: 4273.

41. Kaufman, M.H. 1992. The Atlas of Mouse Development. Academic press, London. 131-133pp.

42. Green, M.C. 1989. Catalog of mutant genes and polymorphic loci. *In* "Genetic variants and strains of the laboratory mouse." (M.F. Lyon, and A.G. Searle, Eds), pp. 12-403, Oxford University Press, Oxford

43. Krumlauf, R. 1994. Hox genes in vertebrate development. *Cell* 78: 191-201

44. Candia, A.F., J. Hu, J. Crosby, P.A. Lalley, D. Noden, J.H. Nadeau, and V.E. Wright. 1992. Mox-1 and Mox-2 define a novel homeobox gene subfamily and are differentially expressed during early mesodermal patterning in mouse embryos. *Development* 116: 1123-1136

45. Hill, R.E., P.F. Jones, A.R. Rees, C.M. Sime, M.J. Justice, N.G. Copeland, N.A. Jenkins, E. Graham, and D.R. Davidson. 1989. A new family of mouse homeobox-containig genes: molecular

structure, chromosomal location, and developmental expression of Hox-7.1. *Genes Dev.* 3: 26-37

46. Hunt, P., M. Gulisano, M. Cook, M.H. Sham, A. Faiella, D. Wilkinson, E. Boncinelli, and R. Krumlauf. 1991. A distinct Hox code for the branchial region of the vertebrate head. *Nature* 353: 861-864
47. Satokata, I., and R. Mass. 1994. Msx1 deficient mice exhibit cleft palate and abnormalities of craniofacial and tooth development. *Nature Genet.* 6: 348-356
48. Chisaka, O., and M.R. Capecchi. 1991. Regionally restricted developmental defects resulting from targeted disruption of the mouse homeobox gene *hox-1.5* . *Nature* 350:473-479
49. De la Cruz, M., C. Sánchez Gómez, M.M. Arteaga, and C. Argüello. 1977. Experimental study of the development of the truncus and the conus in the chick embryo. *J. Anat.* 123:661-686.
50. Noden, D.M. 1991. Origins and patterning of avian outflow tract endocardium. *Development* 111:867-876.
51. Nishibatake, M., M.L. Kirby, and L.H. Van Mierop. 1987. Pathogenesis of persistent truncus arteriosus and dextroposed aorta in the chick embryo after neural crest ablation. *Circulation* 75:255-264.
52. Bockman, D.E., M.E. Redmond, K. Waldo, H. Davis, and M.L. Kirby. 1987. Effect of neural crest ablation on development of the heart and arch arteries in the chick. *Am. J. Anat.* 80:332-341.
53. Sucov, H.M., E. Dyson, C.L. Gumeringer, J. Price, K.R. Chien, and R.M. Evans. 1994. RXRα mutant mice establish a genetic basis for vitamin A signaling in heart morphogenesis. *Genes Dev.* 8:1007-1018.

54. Kinsella, M.K., and T.P. Fitzharris. 1980. Origin of cushion tissue in the developing chick heart: Cinematographic recordings of *in situ* formation. *Science(Wash.DC)*. 207:1359-1360.

55. Fitzharris, T.P., and R.R. Markwald. 1982. Cellular Migration through the cardiac jelly matrix: A stereoanalysis by high voltage electron microscopy. *Dev. Biol.* 92:315-329.

56. Takuwa, N., Y. Takuwa, M. Yanagisawa, K. Yamashita, and T. Masaki. 1989. A novel vasoactive peptide endothelin stimulates mitogenesis through inositol lipid turnover in swiss 3T3 fibroblasts. *J. Biol. Chem.* 264:7856-7861.

57. Ito, H., Y. Hirata, M. Hiroe, M. Tsujino, S. Adachi, T. Takamoto, M. Nitta, K. Taniguchi, and F. Marumo. 1991. Endothelin-1 induces hypertrophy with enhanced expression of muscle-specific genes in cultured neonatal rat cardiomyocytes. *Circ. Res.* 69:209-215.

58. Matsumoto, H., N. Suzuki, H. Onoda, and M. Fujino. 1989. Abundance of endothelin-3 in rat intestine, pituitary gland and brain. *Biochem. Biophys. Res. Commun.* 164:74-80.

59. Masaki, T., J.R. Vane, and P.M. Vanhoutte. 1994. International union of pharmacology nemenclature of endothelin receptors. *Pharmacol. Rev.* 46:137-142.

60. Letterio, J.J., A.G. Geiser, A.B. Kulkarni, N.S. Roche, M.B. Sporn, and A.B. Robbers. 1994. Maternal rescue of transforming growth factor-β1 null mice. *Science* 264:1936-1938.

61. Van Mierop, L.H., and L.M. Kutsche. 1986. Cardiovascular anomalies in DiGeorge syndrome and importance of neural crest as a possible pathogenetic factor. *Am. J. Cardiol.* 58:133-137.

62. Wilson, D.I., I.E. Cross, J.A. Goodship, S. Coulthard, A.H. Carey, P.J. Scambler, H.H. Bain, A.S. Hunter, P.E. Carter,and J. Burn. 1991. DiGeorge syndrome with isolated aortic coarctation and isolated ventricular septal defect in three sibs with a 22q11 deletion of maternal origin. *Br. Heart. J.* 66:308-312.

63. Wilson, D.I., J.A. Goodship, J. Burn, I.E. Cross, and P.J. Scambler. 1992. Deletion within chromosome 22q11 in familial congenital heart disease. *Lancet* 340:573-575.

64. Scamber, P.J., D. Kelly, E. Lindsay, R. Williamson, R. Goldberg, R. Shprintzen, D.I. Wilson, J.A. Goodship, I.E. Cross, and J. Burn. 1992. Velo-cardio-facial syndrome associated with chromosome 22 deletion encompassing the DiGeorge locus. *Lancet* 339:1138-1139.

65. Budarf, M.L., J. Collins, W. Gong, B. Roe, Z. Wang, L.C. bailey, B. Sellinger, D. Michaud, D.A. Driscoll, and B.S. Emanuel. 1995. Cloning a balanced translocation associated with DiGeorge syndrome and identification of a disrupted candidate gene. *Nature Genet.* 10:269-278.

66. Jacks, T., T.S. Shin, E.M. Schmitt, R.T. Bronson, A. Bernards, and R.A. Weinberg. 1994. Tumor predisposition in mice heterozygous for a targeted mutation in *Nf1*. *Nature Genet.* 7:353-361.

67. Buckingham, M. 1994. Molecular biology of muscle development. *Cell* 78:15-21.

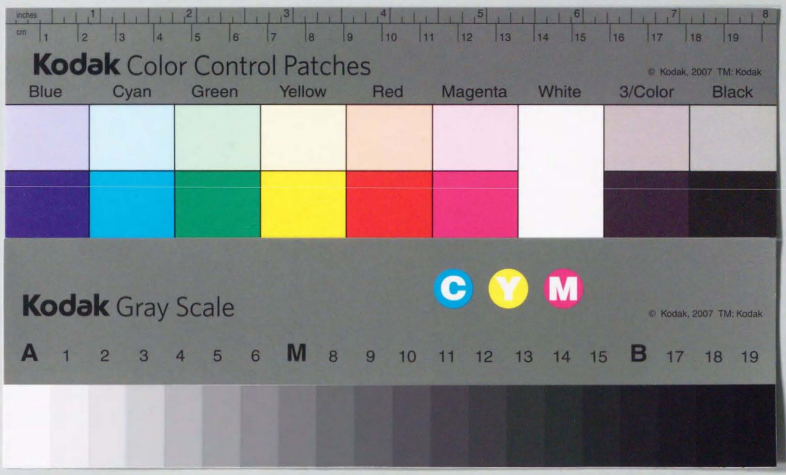
inches
cm
Kodak Color Control Patches
© Kodak, 2007 TM: Kodak
Blue
Cyan
Green
Yellow
Red
Magenta
White
3/Color
Black
Kodak Gray Scale
C
Y
M
© Kodak, 2007 TM: Kodak
A 1 2 3 4 5 6 M 8 9 10 11 12 13 14 15 B 17 18 19